Cornell Prime Dots (C' dots): Ultrasmall PEGylated Fluorescent Core-Shell Silica Nanoparticles for Cancer Theranostics

Honors Thesis
Presented to the College of Agriculture and Life Sciences, Cornell University
in Partial Fulfillment of the Requirements for the
Biological Sciences Honors Program

by
Carlie Mendoza
May 2016

Research Supervisor: Dr. Ulrich Wiesner
Graduate Mentor: Dr. Kai Ma
Department of Materials Science and Engineering, Cornell University

Thesis Advisors: Professors Gerald Feigenson and Volker Vogt

Abstract

Cancer is a prevalent concern in today's society. It is the second most common death in the US, exceeded only by heart disease. Currently, cancer treatment options include surgery, radiation, chemotherapy, hormone therapy, biological therapy, targeted therapy and most recently immunotherapy. Within the past decade, there has been a huge upsurge in novel ideas and technology to combat this disease. From the 2000s, the Wiesner group has been working on silica-based nanomaterials for cancer "theranostics", a combination of diagnostics with therapy. The first generation Cornell dots (CU dots) were fluorescent PEGylated silica nanoparticles used as targeted probes in cancer patient care. These particles have already received FDA-approval and have been tested in first-in-human clinical trials, making them the first inorganic-polymer hybrid diagnostic bio-probes to enter clinical trials. From these limited number of patient trials they can be injected in the body, flow through the bloodstream, and be excreted without noticeable side effects. The purpose of my research was to synthesize the next generation of particles, referred to as C' dots, in aqueous solution thereby preventing volatile organic solvent waste, simplifying the synthesis process, and providing even brighter particles than before. Brighter particles allow for clearer visualization via higher signal to noise ratios in the body, which is especially beneficial when locating, imaging and excising a tumor. This is a valuable component of the particles as they enable more effective treatment of cancer cells, while allowing healthy, living cells to remain unharmed.

Acknowledgements

Foremost, I would like to express my sincere gratitude to my research advisor, Dr. Ulrich Wiesner, for encouraging my interest in nanotechnology as a high school student, and accepting me into his lab after being selected as a Hunter R. Rawlings III Cornell Presidential Research Scholar. This was the opportunity of a lifetime and I am very grateful for the time I have spent conducting this research.

I would like to thank Dr. Kai Ma, my graduate student mentor, for taking me under his wing as a freshman with no background in materials science and engineering, for guiding me these past three and a half years, and challenging me to think outside the box. I have enjoyed our stimulating scientific conversations, resulting from both failed and successful experiments.

I would also like to thank all the members of the Wiesner group. I remember the first time I presented a progress report during a lab group meeting. It was intimidating to speak to a room of 15 graduate students and post-docs who had advanced knowledge on my topic, but I was given constructive criticism and many compliments. I also liked joining in on group lunches and friendly office banter. I really feel like I have a family here, which made going to lab every day that much more enjoyable.

Finally, I would like to thank my family, for their unconditional love and never-ending support. Being away from home was a tough transition, but the memories I've made, the friends I've found, and the opportunities I've received are beyond anything I could have imagined. I will definitely miss "life on the hill."

This work was supported by NIH Grant No. 5R01 CA161280-03. This work made use of the CCMR (supported through the NSF MRSEC program DMR-1120296) and the NBTC shared research facilities at Cornell.

Table of Contents

Introduction

Cancer is a group of diseases characterized by uncontrolled growth and spread of abnormal cells. This can result in death if the spread is not detected and controlled. It is caused by both external factors and internal factors (Kawasaki, 2005). These include tobacco, infectious organisms, chemicals, radiation, inherited mutations, hormones, immune conditions, and mutations that occur from metabolism (Peto, 1983). Currently, cancer is typically treated with surgery, radiation, chemotherapy, hormone therapy, biological therapy, and targeted therapy (Schnipper, 2015). Cancer is a very prevalent concern in today's society. About 1,685,210 new cancer cases were expected to be diagnosed in the U.S. in 2015. This year, about 595,690 Americans are expected to die of cancer, which is more than 1,630 people a day. It is the second most common death in the U.S., exceeded only by heart disease. In the U.S., cancer accounts for nearly 1 of every 4 deaths (American Cancer Society, 2016).

In science today, there have been many recent breakthroughs with nanotechnology, the engineering of functional systems at the molecular scale (Alexis, 2008). 'Nanotechnology' refers to the ability to construct items from the bottom up, producing high performance products on the scale of nanometers (Harper, 2003). There is the possibility of utilizing them in detection, chemotherapy treatments, and initiating apoptosis of cancer cells through gene therapy, targeted gene delivery and gene transfer. Technology that will aid in the detection of cancerous cells, such as the creation of nanosensors, has been constructed at the molecular scale (Peng, 2010). As a promising platform, these materials are extremely sensitive, selective and responsive, and can be used to replace costly and tedious laboratory methods currently in use for monitoring a patient's blood for proteins, chemicals and pathogens (Nie, 2007).

Nanotechnology can also be used in sustained, controlled and targeted chemotherapy (or "personalized chemotherapy"), chemotherapy across various physiological drug barriers, such the gastrointestinal barrier for oral chemotherapy and the blood-brain barrier for treatment of brain tumors and other central nerve system diseases, and eventually, chemotherapy at home (Rahman, 2012). Lastly, targeted gene delivery to selected cell types provides a means for highly specific gene expression. Improved efficiency of gene transfer could be achieved through enhancing the entry of gene vectors into the desired cells and reducing the uptake of the vectors by non-target cells (Labhasetwar, 2005).

Many studies researching the utilization of nanotechnology in the field of oncology are currently ongoing. For example, in an article published in the Clinical Cancer Research journal, the researchers experimented with nanoparticles to be utilized as drug delivery systems. The objective of the nanoparticles was to kill cancer cells more effectively in order to reduce and overcome drug resistance. They also hypothesized how nanoparticles will be developed in the future to improve their therapeutic efficacy and functionality in future cancer treatments (Cho, 2008). Nanoparticles can be made using a variety of materials including polymers, lipids, viruses, and organometallic compounds. For polymer-based drug carriers, the drug is either physically entrapped in or covalently bound to the polymer matrix (Peer, 2007). Polymeric micelles are based on amphiphilic block copolymers, which assemble to form a nano-sized shell structure in aqueous media. The hydrophobic core region collects the hydrophobic drugs and the hydrophilic shell region stabilizes the hydrophobic core and makes the polymers water-soluble, making the particle an appropriate candidate for administration (Nasongkla, 2006). The size of nanoparticles used in a drug delivery system should be large enough to prevent their rapid leakage into blood capillaries, but small enough to escape capture by fixed macrophages that are lodged in the reticuloendothelial

system. Having a hydrophilic surface also helps to evade macrophage capture (Khanna, 2012). Although numerous studies have already been conducted, the rate of translation of nanotechnologies, in particular nanoparticles, into clinical applications is still limited, leaving an abundant amount of future opportunities for exploration.

From the 2000s, the Wiesner group at Cornell has been working on silica-based nanomaterials for cancer "theranostics" (Ow, 2005). The first generation of CU dots were FDA approved for first-in-human clinical trials in 2010, making them the first inorganic-polymer hybrid diagnostic bio-probe to enter clinical trials. Conducted at Memorial Sloan Kettering Cancer Center in NYC during 2011, these nanoparticles were injected in the body of a limited number of cancer patients, flowed through the bloodstream, passed through renal clearance, and were excreted within a couple of hours without noticeable side effects (Phillips, 2014).

The purpose of the present study was to develop a new generation of CU dots, so called Cornell Prime dots (C' dots), with better structure control, brighter fluorescence, higher synthesis purity and improved manufacture reliability. While original CU dots were synthesized in alcohol using the conventional Stöber process, the reaction solvent of C' dots was switched from alcohol to water. This endows the synthesis system with high chemistry versatility. Based on this, new particle compositions have been explored. For example, by integrating aluminum into the silica nanoparticles, aluminum silicate C' dots, so called AlC' dots, were synthesized to further increase particle fluorescence brightness. Finally, efficient incorporation of highly negatively charged NIR emitting fluorophores was achieved.

Materials and Methods

Materials

Dimethyl sulfoxide (DMSO), isopropanol, (3-mercaptopropyl) trimethoxy-silane (MPTMS), tetramethyl orthosilicate (TMOS), tetraethyl orthosilicate (TEOS), aluminum-tri-sec-butoxide (ASB), 2.0 M ammonia in ethanol and 27 wt % ammonium hydroxide were purchased from Sigma−Aldrich. 2-[methoxy (polyethyleneoxy)6-9propyl]trimethoxysilane (PEG-silane, molar mass of ~500 g/mol) was purchased from Gelest. Cy5 and Cy5.5 florescent dyes were purchased from GE Healthcare Life Sciences. Deionized (DI) water was generated in the shared Nanobiotechnolgy Center (NBTC) lab using a Millipore Milli-Q system.

Methods

The following protocols were adapted from previous work in our lab. The C' dot protocol follows the same steps as the CU dot protocol previously published, except for the synthesis of the silica precursors and the ability to add multiple silica shells while remaining under 10 nm (Ow, 2005; Burns. 2009).

Synthesis of sub-10 nm PEGylated silica nanoparticles

This synthesis protocol spans 7 days. First, a mixture of 0.02 M $NH_3 \bullet H_2O$ is made by combining 100 μL of 2.0 M ammonia aqueous solution with 10 mL of DI water in a small glass vial. The mixture is vortexed for 10 seconds and should be transparent. In a small, round bottom flask, 1 mL of this mixture is added to 9 mL of DI water. On a stir plate at room temperature, 0.43 mmol of TMOS is added and left overnight. Next, 0.21 mmol of PEG-silane is added to the solution, while stirring overnight. Then, the flask is placed in a static, hot oil bath set at 80°C for 24 hours. Next, the solution is cooled to room temperature and transferred to dialysis tubing (Pierce brand) with a 10,000 molecular weight cut-off (MWCO). The sample is set in a large 2000 mL

beaker filled with DI water. The water is changed once per day for 2 additional days to wash away any remaining reagents, such as free-floating PEG. After dialysis, the sample is removed from the tubing and filtered through a 0.2 μM syringe filter (Fisher brand) to remove aggregate particles or dust present in the solution. The protocol results in a 10 mL sample, containing blank core silica nanoparticles. Stored in a 20 mL glass vial at room temperature, the solution can undergo further characterization.

Synthesis of sub-10 nm PEGylated fluorescent silica nanoparticles

This synthesis protocol spans 8 days. First, Cy5 or Cy5.5 dye with maleimido functionality is conjugated to MPTMS in DMSO. The molar ratio of fluorophore to MPTMS is equal to 1:25. After 24 hours, this conjugated dye is added to the stirring solution of DI water, 0.02 M $NH_3 \bullet H_2O$, and TMOS. The protocol continues as previously described, with the addition of PEG-silane, heat treatment in a hot oil bath, dialysis and syringe filtering. This results in a 10 mL sample, containing fluorescent core silica nanoparticles.

Synthesis of sub-10 nm PEGylated core-shell silica nanoparticles and sub-10 nm PEGylated fluorescent core-shell silica nanoparticles

This synthesis protocol spans 10-11 days. Following the previously described protocols, core-shell nanoparticles can be synthesized with blank or fluorescent cores. After the mixture of DI water, 0.02 M $NH_3 \bullet H_2O$, and TMOS (with or without conjugated dye) is left stirring overnight, the solution is transferred to a large, round bottom flask and diluted by adding 40 mL of DI water. Then, 10 mL of this large batch is aliquoted into a small, round bottom flask and continues onto the PEGylation step. Addition of a single silica shell is achieved by dosing the stirring solution with a mixture of TEOS and DMSO, with a volume ratio of 1:4, using the Eppendorf Electronic Dispensing System. The system is set to dispense 10 μL every 15 minutes, eighty times. This step

is repeated until the desired layers of shells are added. In this case, we added up to 4 shells. To keep the pH at neutral for optimized reaction kinetics, ~2 mL of 0.02 M M $NH_3 \bullet H_2O$ was added to the solution after the addition of 2 layers. This was monitored using color-changing pH paper. The protocol results in five, 10 mL samples, containing silica nanoparticles with 0, 1, 2, 3, or 4 shells.

Synthesis of sub-10 nm PEGylated aluminosilicate nanoparticles and sub-10 nm PEGylated fluorescent aluminosilicate nanoparticles

This synthesis protocol spans 7-8 days. First, a mixture of 0.043 mmol of ASB is made in a small glass vial by dissolving a volume ratio of 1:9 ASB and isopropanol. In a small, round bottom flask, 9.6 mL of DI water is mixed with 400 μL of 0.5 M HCl. After stirring for 3 minutes, 0.43 mmol of TMOS and the 0.043 mmol of ASB are added. Thirty minutes later, 0.21 mmol of PEG-silane is added and the solution is switched back to neutral pH by adding ~140 μL of 27 wt% ammonium hydroxide. The next day, the flask if transferred into a hot oil bath set at 80°C for 24 hours. Similar to the previously described protocols, the solution is transferred to dialysis tubing with a 10,000 MWCO, the DI water is changed two additional times, and then the solution is filtered through a 0.2 μM syringe filter. This results in a 10 mL sample, containing blank or fluorescent core aluminosilicate nanoparticles.

Synthesis of sub-10 nm PEGylated core-shell aluminosilicate nanoparticles and sub-10 nm PEGylated fluorescent core-shell aluminosilicate nanoparticles

This synthesis protocol spans 10-11 days. Following the previously described protocols, a large batch of core-shell aluminosilicate nanoparticles can be synthesized with blank or fluorescent cores. Additional layers of silica are added to aliquots of the solution using the Eppendorf Electronic Dispensing System. After these additions, the synthesis continues as before. However,

0.21 mmol PEG with a molar mass of ~400 g/mol is added instead of PEG-silane. Then the pH is tuned back up to neutral, 0.21 mmol PEG-silane is added, heat treatment is applied, the solution is dialyzed and then syringe filtered. This results in five, 10 mL samples, containing aluminosilicate nanoparticles with 0, 1, 2, 3, or 4 shells.

Characterization of particle morphology by dynamic light scattering

Hydrodynamic particle sizes and size distributions were measured by dynamic light scattering (DLS), using a Malvern Zetasizer Nano-SZ. This machine is located in the NBTC lab in Duffield Hall. In a plastic cuvette, 1 mL of each sample was measured three times at 20 °C and the average diameter of each sample was calculated by averaging the mean diameters.

Characterization of particle morphology by transmission electron microscopy

To obtain transmission electron microscopy (TEM) images, the FEI Tecnai T12 Spirit microscope was operated at an acceleration voltage of 120 keV. This microscope is located on the first floor of Duffield Hall. 10 μL of silica nanoparticles, diluted 1:10 into absolute ethyl alcohol, were dropped onto a 150 mesh copper grid with carbon film backing, and dried in air.

Characterization of fluorophore encapsulating particles by spectrophotometry

Absorbance spectra of samples were measured by a Varian Cary Model 5000 spectrophotometer. First, the concentrations of the samples were systematically varied, so that the absorbance spectra were matched. Since absorbance and optical density are directly related, matching the absorbance adjusted the optical density so they were the same for the different samples. Then, the absorbance-matched samples were subjected to emission scans using a Photon Technologies International Quantamaster spectrofluorometer. To calculate the quantum efficiency enhancement, the peak intensity of emission spectra of the particles was divided by the peak intensity of the absorption-matched solution of free dye.

Characterization of fluorophore encapsulating particles by fluorescence correlation spectroscopy

Fluorescence correlation spectroscopy (FCS) was measured using a home-built FCS setup in the sub-basement of Bard Hall. A 633 nm solid-state laser was used as the laser source for the Cy5 and Cy5.5 fluorophores. From the FCS autocorrelation curves, the hydrodynamic size, brightness per particle, and particle concentration were obtained. Then, to calculate the number of fluorophores per particle, the particle concentration obtained from FCS was divided by the fluorophore concentration that was obtained from the absorbance measurements.

Results and Discussion

Controlled fluorescent core silica nanoparticle growth

Though the synthesis of these core silica nanoparticles was previously published by members of the Wiesner group, it was necessary for this researcher to be able to successfully reproduce the results before optimizing the protocol for silica shell additions.

Figure 1 is an illustration of the composition of a C' dot. As previously detailed in the Methods section, sub-10 nm diameter silica nanoparticles are synthesized in DI water at room temperature, with TMOS as the silica source and ammonium hydroxide as the base catalyst. After formation of the particles, particle growth is terminated with the addition of PEG-silane to the reaction. Heat treatment in a hot oil bath is followed by several days of dialysis and syringe filtering to clean the particles. These final two steps are necessary for removing unreacted reagents and aggregated particles.

The synthesis protocol outlined is similar to the conventional Stöber method. The Stöber synthesis of colloidal silica was first described in 1968, and can yield monodisperse nano- to micro-meter sized silica nanoparticles. However, instead of alcohol as the reaction solvent, water was used. This lead to better-defined reaction kinetics for ultrasmall silica nanoparticle growth.

Although the hydrolysis rate of TMOS is greatly increased in water relative to alcohol, homogenous particles were still synthesized at high concentrations. This switch to water allows for the translation of these stable particles to biological applications by decreasing the exposure to toxic materials. Furthermore, termination of particle growth by PEG-silane addition provides another synthesis parameter by which particle size can be precisely controlled and final stability can be enhanced.

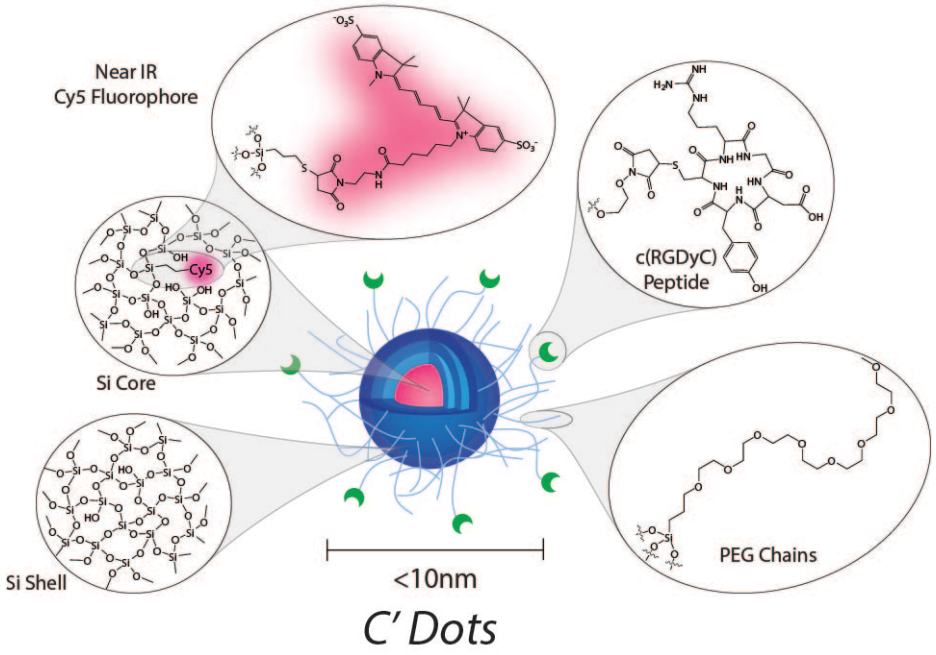

Figure 1: Illustration of a C' dot's composition, which consists of a silica core and near IR Cy5 fluorophores encapsulated in silica shells and covered in PEG chains and c(RGDyC) peptides

Controlled fluorescent core-shell silica nanoparticle growth

This section took up the majority of the time spent on this project. Optimization of the protocol for core-shell synthesis involved manipulating many variables. Some of these included the silica precursor used, the pH of the system, the concentration of the solution, the concentration of silica in each dose, the amount of doses per shell, and the amount of lag time between doses.

Figure 2 shows an illustration of the core-shell synthesis pathway. Deposition of additional silica shells was achieved by dosing the reaction with a mixture of TEOS and DMSO. The dosed silane would further condense onto the existing core particles after hydrolysis. This resulted in additional silica layers surrounding the cores.

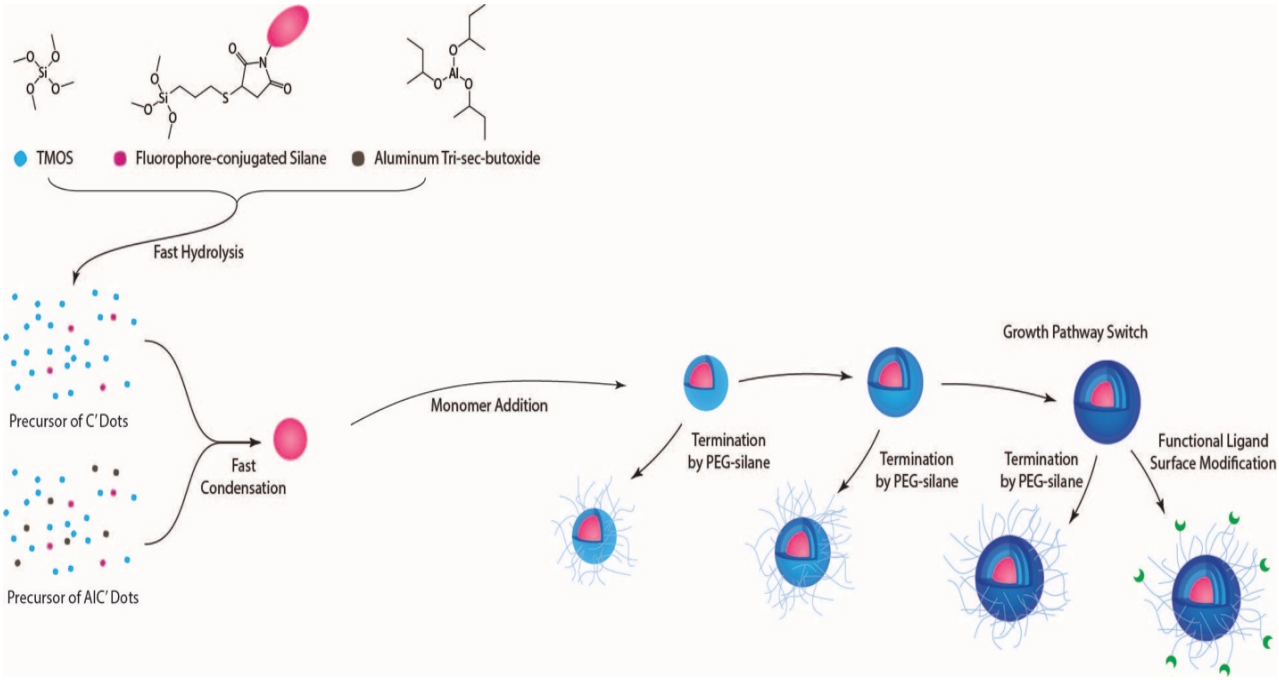

Figure 2: Illustration of the core-shell synthesis, which is water-based and yields blank or fluorescent silica nanoparticles after doping the solution with additional silica

Initially, silica shell addition was attempted with TMOS. Early results indicated that simply dosing TMOS into the solution does not result in particle size increase. Shown in figure 3 is the DLS measurement of blank C' dots with 2 shells, with an average size of ~3-4 nm. It is most likely that secondary nucleation, instead of condensation onto the existing particles, occurred due to the fast hydrolysis and condensation rates of TMOS in water.

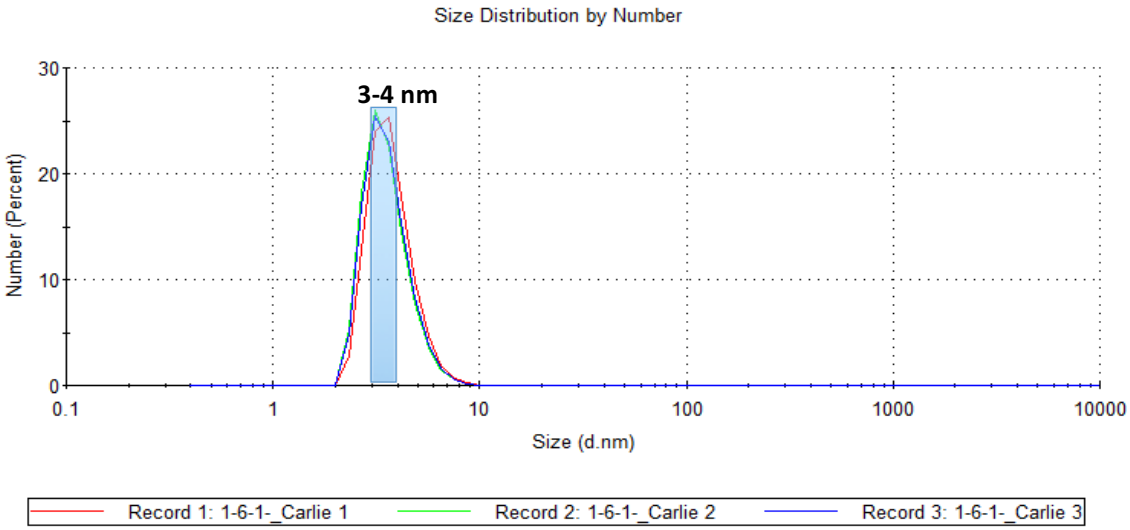

Figure 3: DLS measurements of blank C' dots with 2 TMOS shells. The Malvern Zetasizer recorded three measurements, each with 10 runs. The curves were superimposed and determined the particles were roughly 3-4 nm on average, which was inconsistent with the expected results.

In order to overcome this challenge, TEOS was used instead of TMOS for silica shell addition. Structurally similar to TMOS, TEOS has a slower hydrolysis rate. After optimizing the conditions previously listed, the hydrolysis of TEOS was tuned to be slightly slower than the time required for a single dose to thoroughly mix with the entire solution. This allowed the TEOS dose to spread out into the solution, hydrolyze, and then condense onto the existing particles, instead of forming secondary particles.

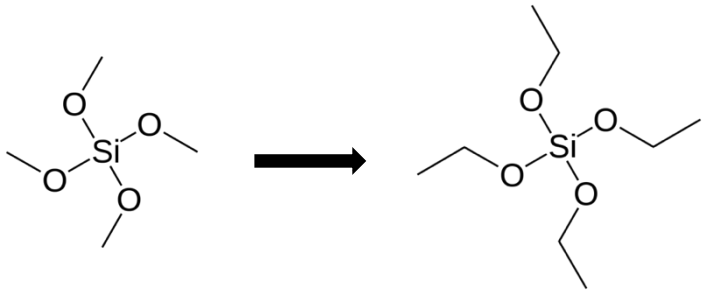

Blank core-shell silica nanoparticles were first synthesized using this protocol, resulting in a core size of ~ 4 nm. Three shells were added, giving particle sizes of 5.6 nm (1 shell), 6.5 nm (2 shells), and 7.8 nm (3 shells). This was determined by TEM imaging, shown in figure 4, and confirmed by DLS measurements, shown in figure 5. After repeatable results were obtained successfully, the experiment was conducted with Cy5 dye-containing cores.

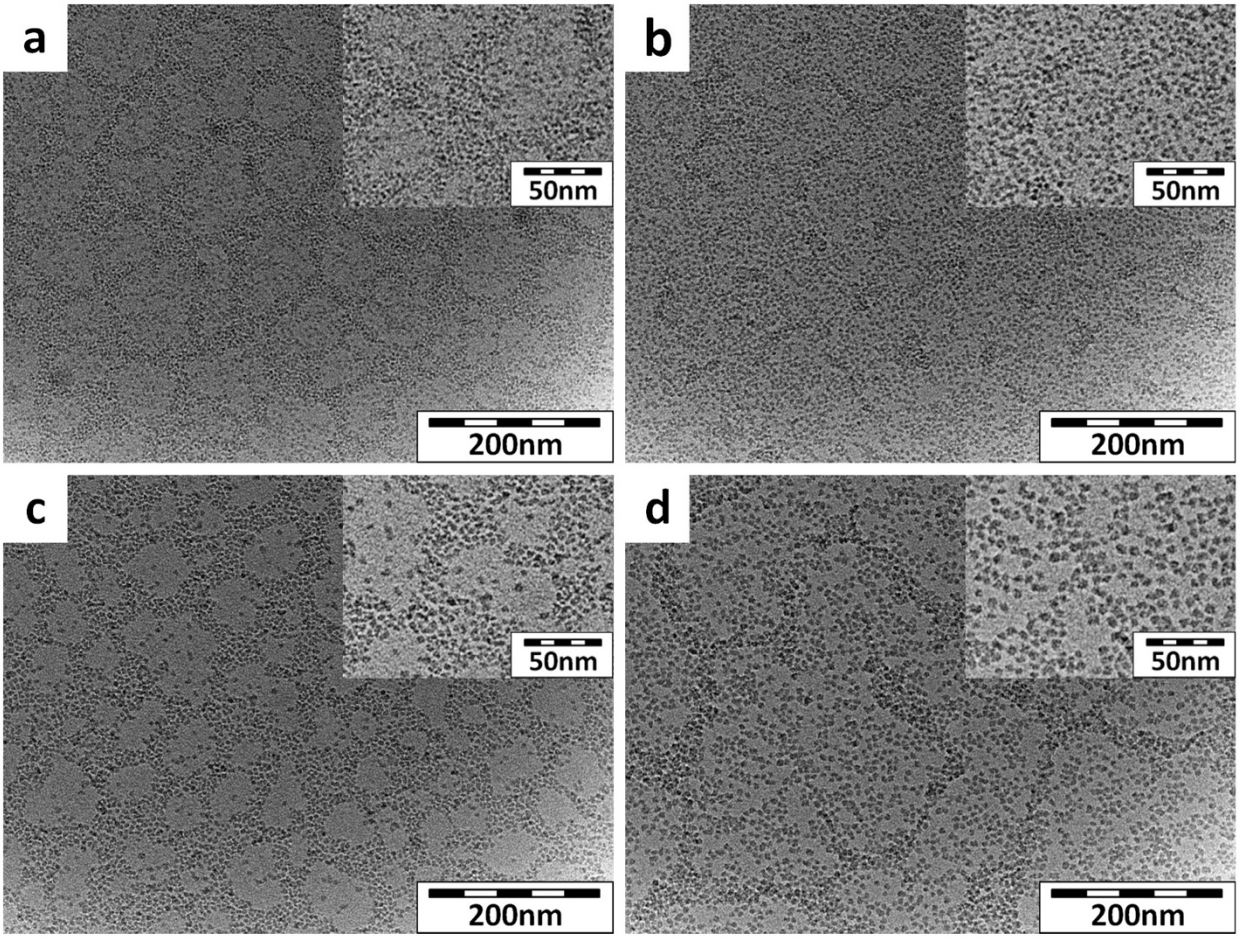

Figure 4: TEM images of blank silica nanoparticles with TEOS shells at two different magnifications (50 and 200 nm scale bars); (a) core, (b) 1 shell, (c) 2 shells, (d) 3 shells. An increase in diameter is observed as silica shells are added. In the images taken at a lesser magnification, the particles do not appear to be uniformly distributed. This apparent network pattern of particles is due to the sample preparation, resulting from capillary forces acting on the particles during water evaporation (images were obtained with the aid of Dr. Kai Ma).

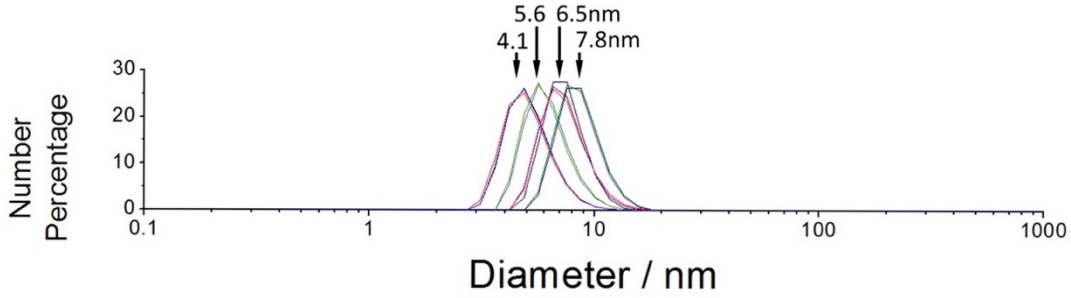

Figure 5: DLS measurements of C' dot size; core = 4.1 nm, 1 shell = 5.6 nm, 2 shells = 6.5 nm, 3 shells = 7.8 nm (images were obtained with the aid of Dr. Kai Ma).

Fluorescent particles allow for visualization when applied to cancer diagnostics. Figure 6 shows the TEM images of these fluorescent C' dots. By adding 1-4 silica shells to 5-nm-sized Cy5 doped core particles, the diameter increases by <1 nm, which is the size of one single SiO_2 unit in the particles. These data imply that the synthesis results in precise size control close to the atomic layer level.

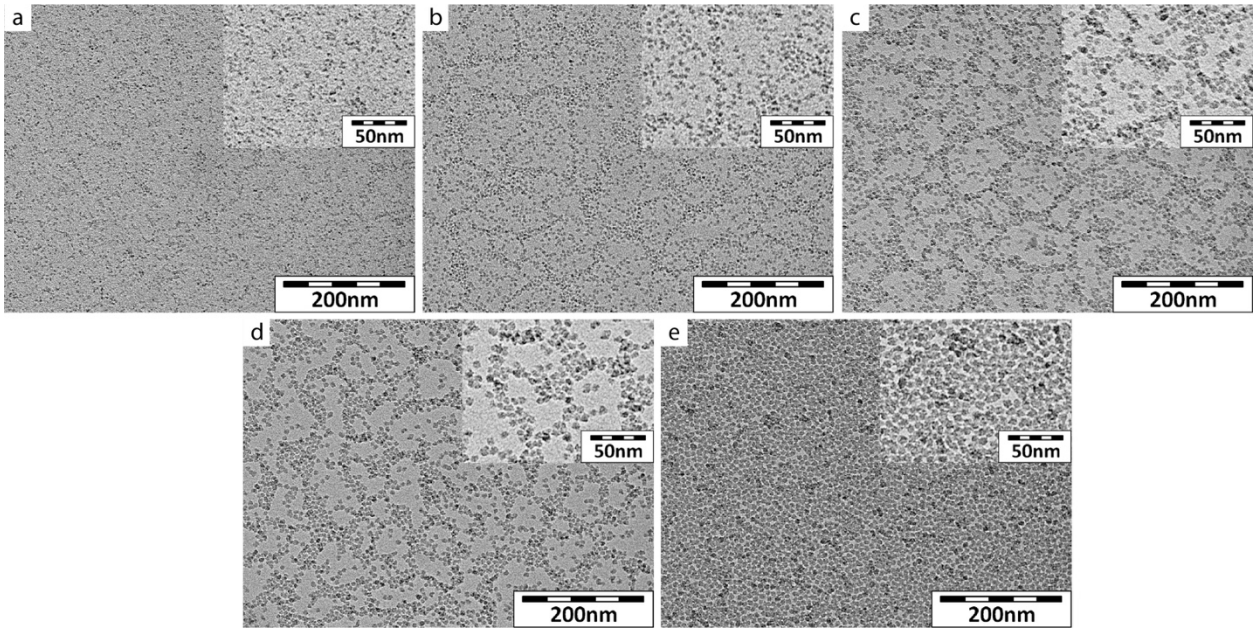

Figure 6: TEM images of Cy5-encapsulated fluorescent silica nanoparticles at two different magnifications, 50 nm and 200 nm; (a) core, (b) 1 shell, (c) 2 shells, (d) 3 shells, (e) 4 shells

Figure 7 shows the absorbance and emission spectra of the core-shell silica nanoparticles, compared to free Cy5 dye. The varied sample concentrations were systematically diluted to the same concentration through matching their absorbance values. The emission from the absorbance matched samples increased when additional silica shell was added. Typically, the fluorescent cores have dye molecules not fully incorporated in the rigid network. When absorbing energy, some is transferred into interatomic forces, such as vibrations or bond rotations. As a result, the emitted energy is less than maximal. The observed increase in emission indicates that the extra silica layers enhance the quantum yield of the Cy5 dye through better encapsulation of the dyes inside the

particles. This increased brightness is desirable because it will allow more distinctive labeling with enhanced signal to noise ratios when imaging tumors in the body.

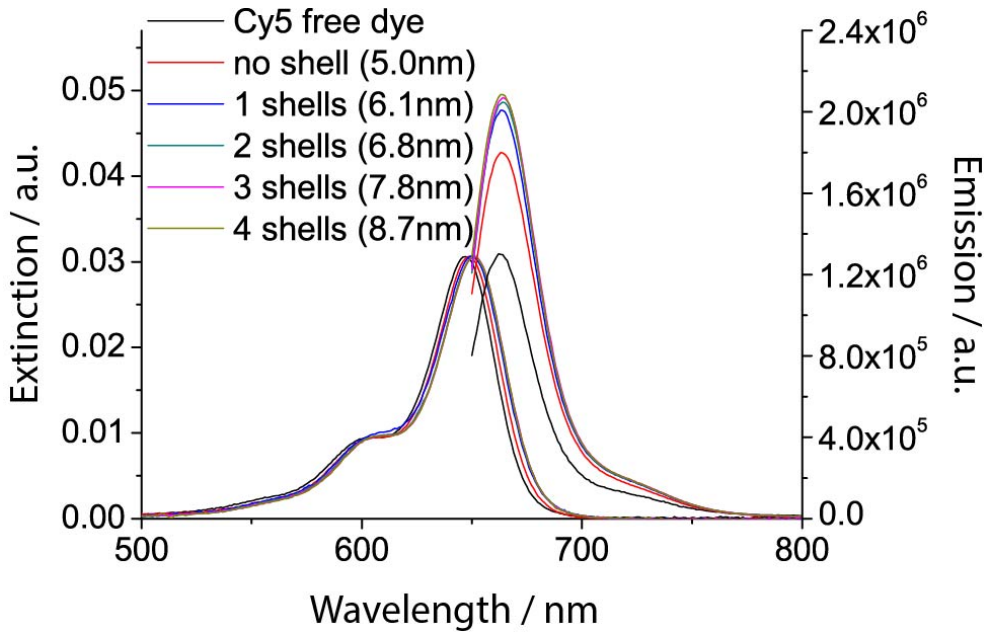

Figure 7: Absorbance-matched (left set of curves) and emission spectra (right set of curves with different peak heights) of core-shell silica nanoparticles measured by a spectrophotometer (measurements were obtained with the aid of Dr. Kai Ma).

Figure 8 is an illustration of our home-built FCS setup. FCS, which stands for fluorescence correlation spectroscopy, is a correlation analysis of fluctuations of the fluorescence intensity. The technique is extremely useful when working with fluorescent nanoparticles. It can be used to measure several characteristics of the fluorescent probe in a single run. The autocorrelation function G(τ) is defined as: $$G(\tau) = \frac{\langle \delta F(t) \delta F(t+\tau) \rangle}{\langle F(t) \rangle^2}$$

where F(t) is the fluorescence obtained from the volume at time t; τ is the delay, and δF(t) = F(t) - <F(t)> is the deviation from the mean fluorescence. Based on the calculation formula and the graphed values, the addition of silica shells results in a shift in the autocorrelation curves to the right, shown in figure 9. This tells us that there is slower diffusion, implying that the particles are increasing in size, which supports both the TEM and DLS data.

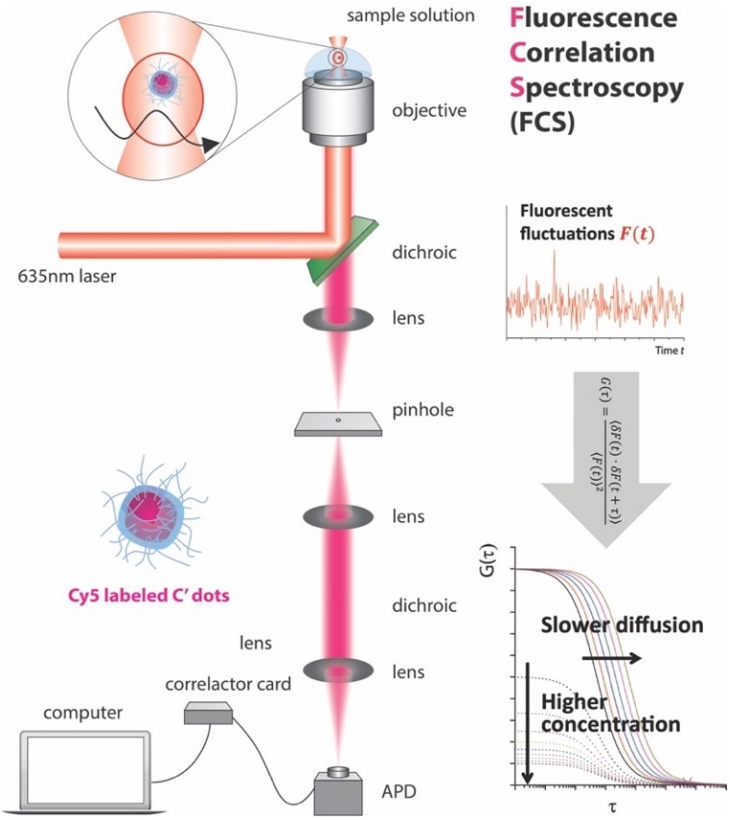

Figure 8: Illustration of the home-built FCS setup

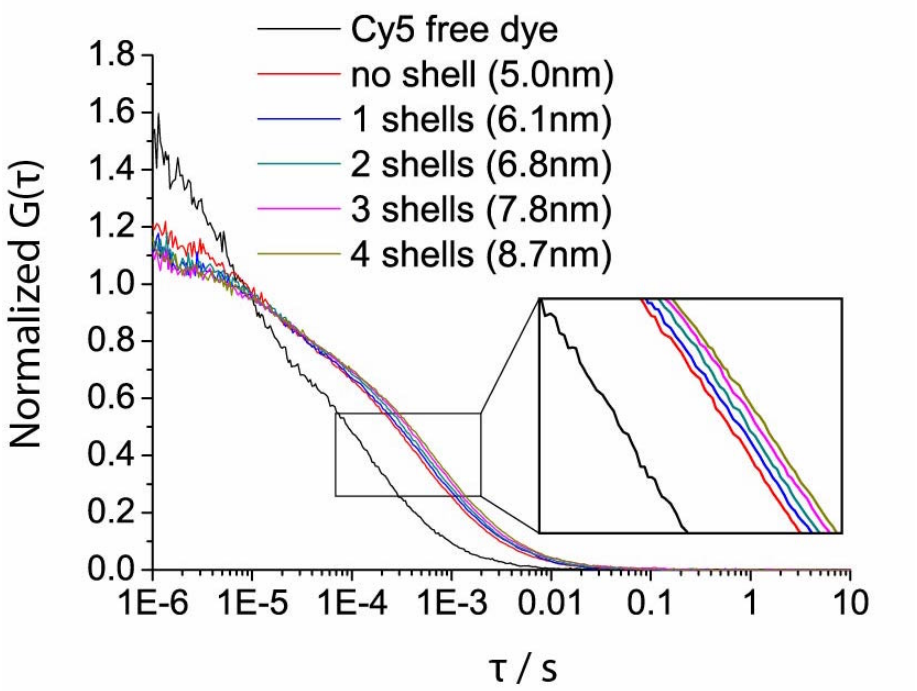

Figure 9: FCS autocorrelation curves of core-shell silica nanoparticles (measurements were obtained with the aid of Dr. Kai Ma).

The FCS autocorrelation curves, G(τ), can tell us the number of diffusing species, N, based on the value of G(τ) at τ=0, which is proportional to 1/N, and the number of photons collected from the volume can tell us the average count rate per diffusing species. This in turn, allows determination of the number of dyes per particle (Figure 10) and brightness per particle. Figure 11 suggests there is a quantum enhancement over free Cy5 dye, which increases from ~1.3 for the core particle to ~1.7 as the number of silica shells increases from 0 to 4. Quantum efficiency enhancement is determined from the difference of fluorescence intensity peak heights relative to free dye. Though there is no obvious trend in increased number of dyes per particle, enhancement of brightness per dye results in an increase of particle brightness.

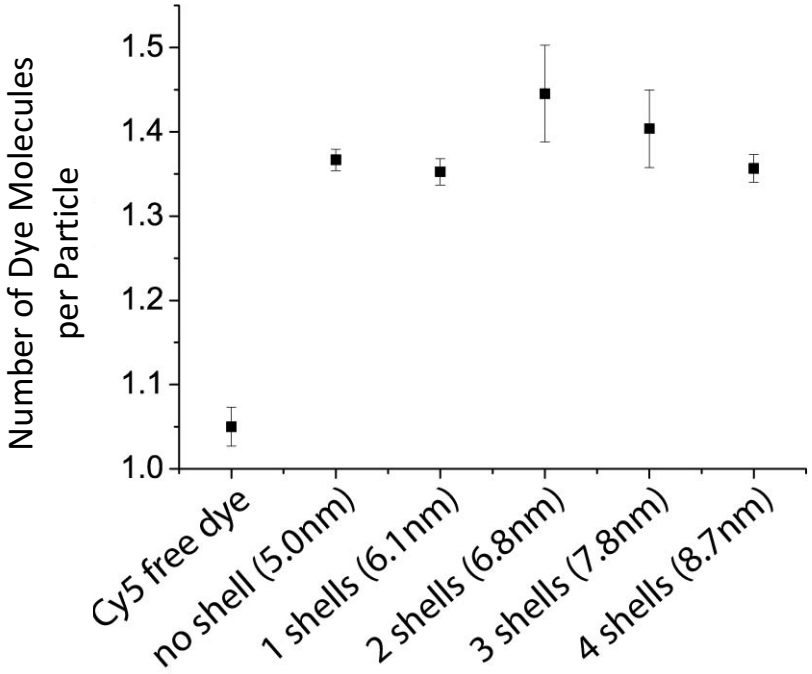

Figure 10: Number of dye molecules per silica nanoparticle based on FCS measurements. Because these are relative measurements, the data point for Cy5 free dye is not 1.0. Systematic variation comes from the absorbance and emission measurements (measurements were obtained with the aid of Dr. Kai Ma).

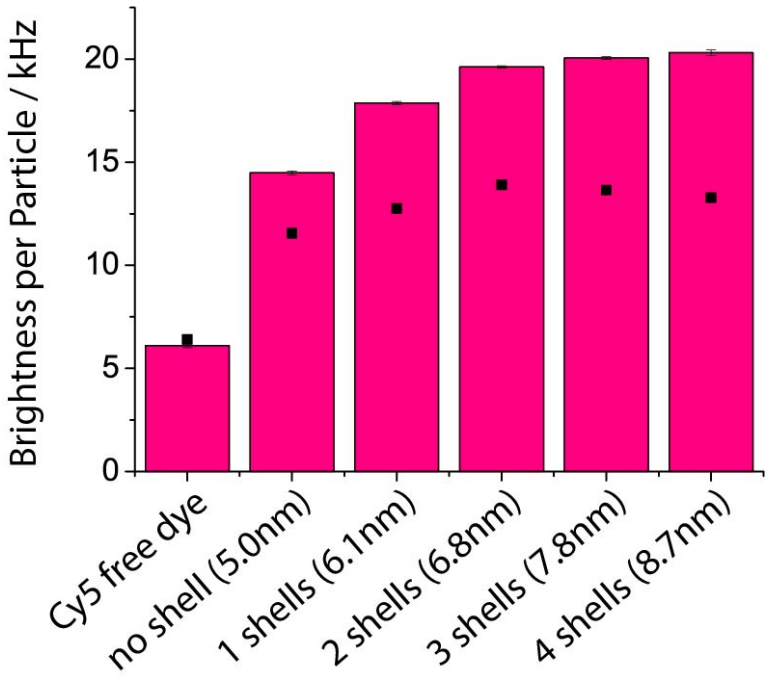

Figure 11: Calculated fluorescence per particle is represented by the black dots. Measured fluorescence brightness per particle is represented by the columns. The disparity in calculated and measured fluorescence is a result of systematic error. The explanation for this disparity is unknown. Statistical error was not significant, evident from small error bars. (measurements were obtained with the aid of Dr. Kai Ma).

Controlled fluorescent silica nanoparticle growth with different inorganic compositions

The motivation for incorporating other inorganic compositions was the limitation of fluorophore incorporation with emission spectra further out into the Near Infrared (NIR) into our C' dot silica nanoparticles. Typically, these fluorophores have larger molar mass and size, requiring more negatively charged sulfate groups on the periphery to generate water solubility. Since silica above its isoelectric point of pH > 2.7 is also negatively charged, strong electrostatic repulsive interactions make covalently encapsulating such highly negatively charged NIR fluorophores into silica nanoparticles challenging.

Figure 12 is an illustration of the composition of an Al C' dot. Shown in the Si-Al core is a model of the molecular structure of the aluminosilicate core. Shown in the model is an NIR Cy5.5 dye covalently encapsulated in the network. As previously detailed in the Methods section, sub-

10 nm diameter aluminosilicate nanoparticles are synthesized in DI water at room temperature, with ASB as the aluminum precursor, TMOS as the silica source and HCl as the acid catalyst. For the addition of silica shells, PEG chains of ~400 g/mol are first added, and then the pH of the solution is increased. After formation of the particles, particle growth is terminated with the addition of PEG-silane to the reaction. Heat treatment in a hot oil bath is followed by dialysis and syringe filtering to clean the particles, removing reaction reagents and aggregated particles.

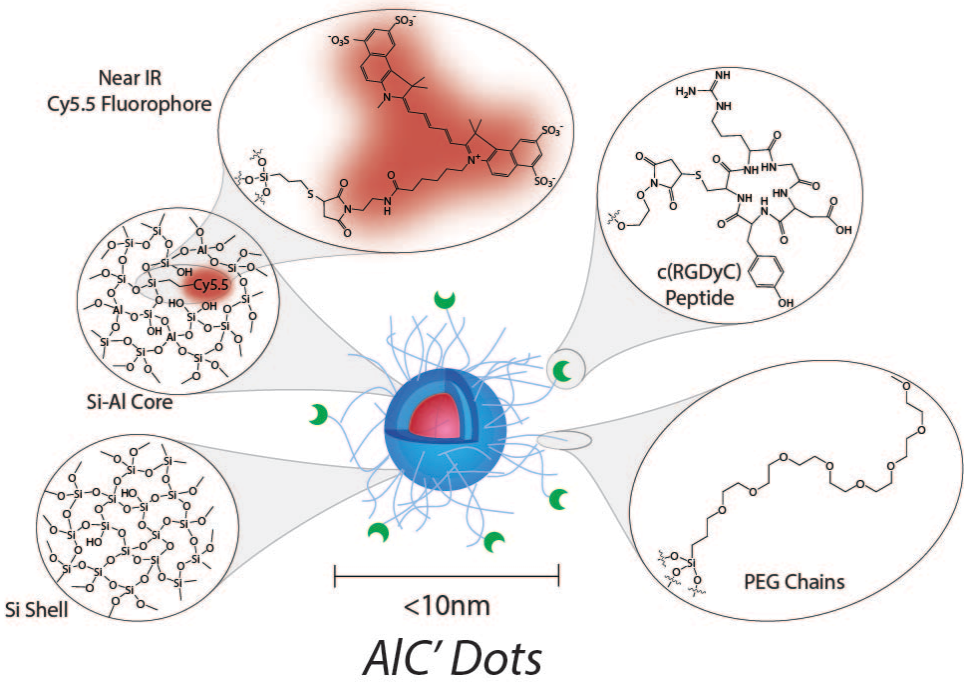

Figure 12: Illustration of an Al C' dot's composition, which consists of an aluminosilicate core and near IR Cy5.5 fluorophores encapsulated in silica shells and covered in PEG chains and c(RGDyC) peptides

First, blank core-shell aluminosilicate nanoparticles were synthesized using this protocol, resulting in a measured core size of ~ 3.5 nm by DLS. TEM imaging resulted in core size measurements of ~5 nm. Both of these are shown in figure 13. Once two shells were successfully added, the synthesis was repeated using Cy5.5 dye-containing cores. By adding 2 silica shells, the diameter increases by ~4 nm, which is shown in figure 14.

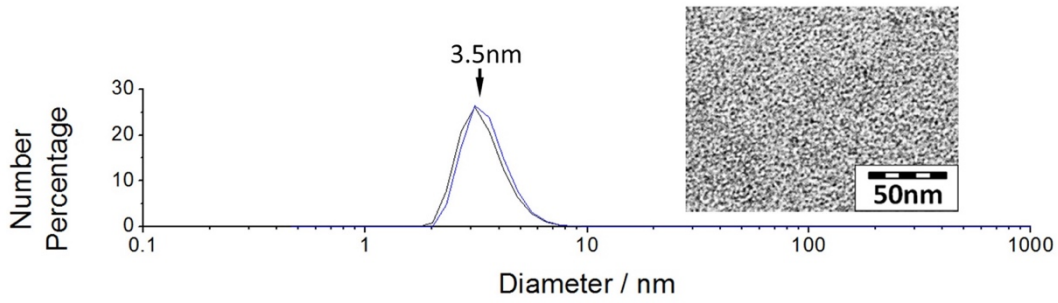

Figure 13: DLS measurement and TEM image of blank core aluminosilicate nanoparticles

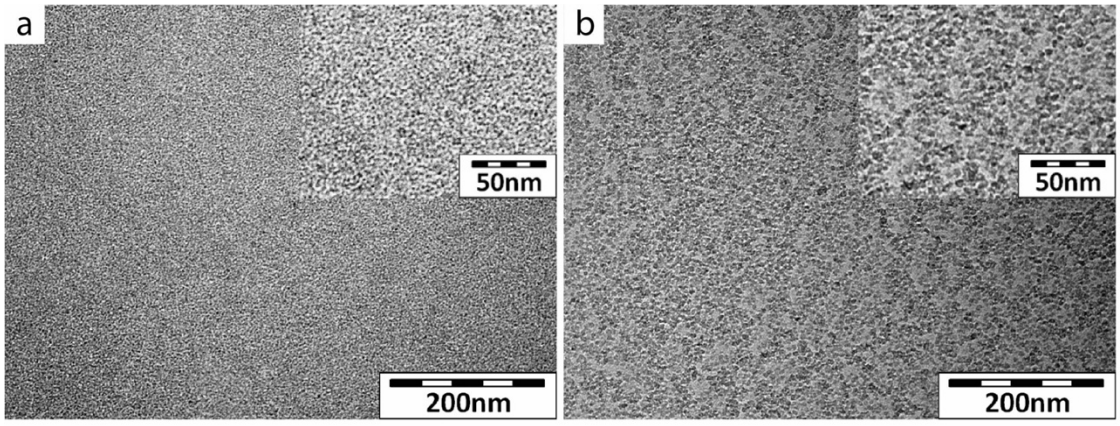

Figure 14: TEM images of aluminosilicate nanoparticles; (a) core, (b) 2 shells (images were obtained with the aid of Dr. Kai Ma).

Once the conditions were optimized, the synthesis was applied to fluorescent particles. Figure 15 shows the absorbance and emission matched spectra of the core-shell aluminosilicate nanoparticles, compared to free Cy5.5 dye. Based on the graphs, the addition of shells significantly increased the quantum yield of Cy5.5 dye. Analysis of the data indicates that these dots have a quantum enhancement over free dye of 2.6, which is significantly larger than the 1.7 obtained for the core only.

Additionally, the FCS autocorrelation curve shown in figure 16 implies that there is an increase in particle size, supporting both the TEM and DLS data. Similar to the reasoning for increased brightness due to increased rigidity of the core-shell silica nanoparticles, the incorporation of aluminum into the silica network also enhances its rigidity. Another contributing

factor may be a decrease in quenching, which is the loss of fluorescence signal due to short-range interactions between the fluorophore and the local environment, or between nearby fluorophores. The regular pattern of the aluminosilicate matrix with covalently linked dye, as well as encapsulation of the core, are two ways of ensuring optimized brightness per particle.

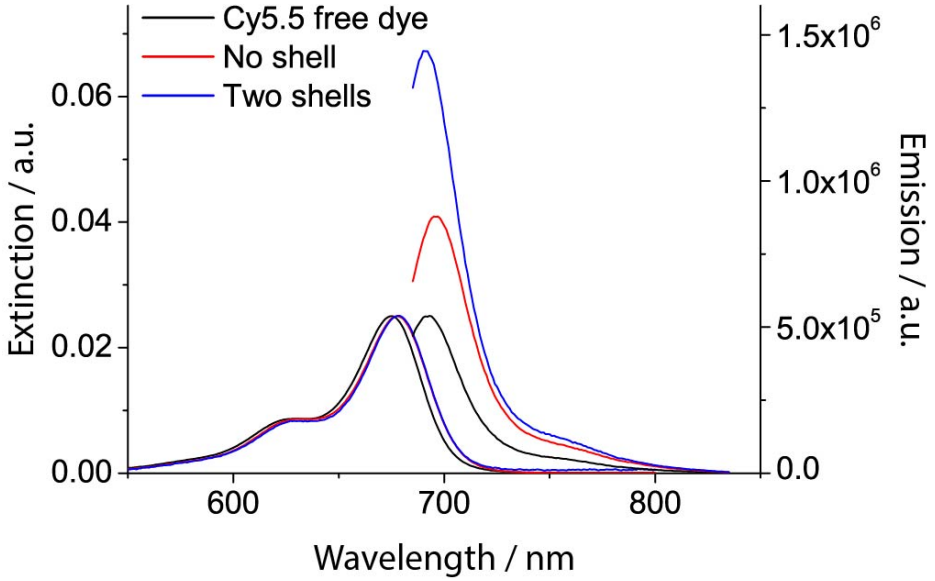

Figure 15: Absorbance-matched (left set of curves) and emission spectra (right set of curves with different peak heights) of core-shell aluminosilicate nanoparticles measured by a spectrophotometer (measurements were obtained with the aid of Dr. Kai Ma).

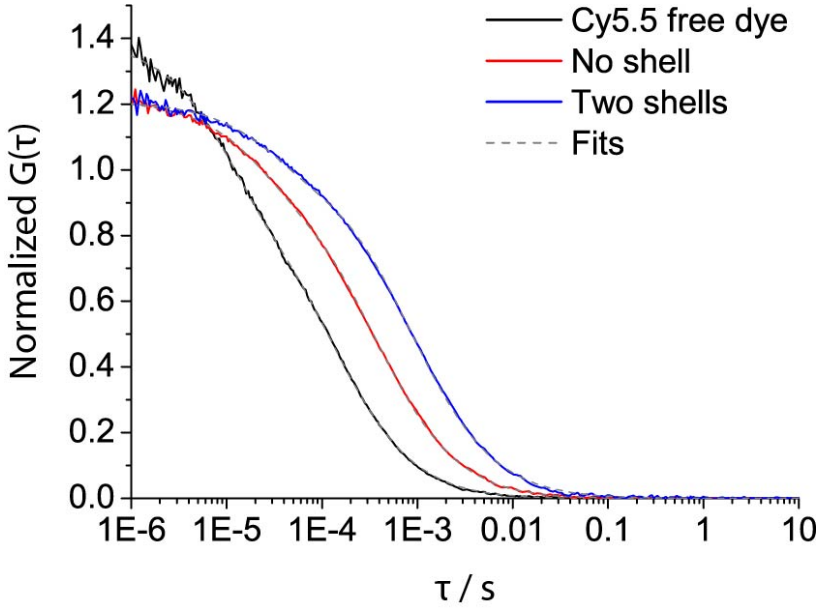

Figure 16: FCS autocorrelation curves of core-shell aluminosilicate nanoparticles (measurements were obtained with the aid of Dr. Kai Ma).

Biological Implications and Future Work

The research conducted by this author contributed to the development of ultrasmall, PEGylated, fluorescent core-shell silica nanoparticles. Compared to the original CU dot synthesis conducted with ethanol as the solvent, the C' dot synthesis yields unprecedented control, especially below 10 nm. Controlled particle size and distribution is important for medical application. For example, sub-10 nm particles ensure effective renal clearance. These water-based nanoparticles have three important advantages:

Firstly, synthesis in water is ideal if we want to commercialize this product in the future. Using water as the solvent is more environmentally friendly, especially if conducted on a large scale. Scaling up the batch size will require a significant amount of ethanol. Cost of manufacture is increased with the need to purchase these chemicals in bulk and dispose of hazardous waste materials.

Secondly, producing water-based nanoparticles is more highly desired for the translation to clinical application. Because these materials are intended for nanomedicine, using ethanol as the solvent raises questions of possible toxicity when injected in the body. To decrease this possibility, the particles undergo extensive cleaning processes, which are also costly. Eliminating this issue results in decreased cost and safer materials.

Lastly, the development of a water-based system opens the door to more versatile chemistry. In biology, reactions occur where water is the solvent. For example, diatoms, one of the most common type of phytoplankton, produce silica exoskeletons. Biosilica synthesis has become of increasing interest, especially in its application to chemical and pharmaceutical processes. Combined with this knowledge, our system has potential to be used for synthesizing all sorts of silica-based nanomaterials.

Additionally, fluorescence microscopy is usually the preferred method of choice for observing processes in living systems. Some of its advantages include its non-invasive utilization and sensitivity to subtle changes in biological processes. With the next generation of C' dots being synthesized in water and to be even brighter particles than before, they hold a promising future for biological application and commercialization. These "ultrabright" and "ultrasmall" C' dots are now being used in human clinical trials at Memorial Sloan Kettering Cancer Center, involving melanoma and brain cancer patients. The initial results are encouraging. Because C' dots specifically target cancerous cells, they can serve as distinctive markers for surgeons during an operation.

Through the work that has been conducted over the past couple of years, some limitations of these nanoparticles have already been encountered. The current project being pursued is the synthesis of other ultrasmall structures based on the non-traditional Stöber synthesis detailed here. Hopefully, these will result in nanoparticles that can serve as a robust cancer drug-delivering platform, with high specificity targeting cancerous cells.

Published Findings

Ma, K., Mendoza, C., Hanson, M., Werner-Zwanziger, U., Zwanziger, J., Wiesner, U (2015). Control of Ultrasmall Sub-10 nm Ligand-Functionalized Fluorescent Core–Shell Silica Nanoparticle Growth in Water. *Chemistry of Materials 27*(11) (May 2015): 4119-4133.

Citations

Alexis, F., Rhee, J., Richie, J., Radovic-Moreno, A., Langer, R., & Farokhzad, O. (2008). New frontiers in nanotechnology for cancer treatment. *Urologic Oncology: Seminars and Original Investigations, 26*(1), 74-85.

Burns, A., Vider, J., Ow, H., Herz, E., Penate-Medina, O., Baumgart, M., Larson, S., Wiesner, U., & Bradbury, M. (2009). Fluorescent silica nanoparticles with efficient urinary excretion for nanomedicine. *Nano Letters, 9*(1), 442-448.

Cho, K., Wang, X, Nie, S., Chen, G., & Shin, M. (2008). Therapeutic nanoparticles for drug delivery in cancer. *Clinical Cancer Research 14*(5)*,* 1310-1316.

Harper, T. (2003). What is nanotechnology?. *Nanotechnology, 14*(1). doi: 10.1088/0957-4484/14/1/001

Kawasaki, E., & Player, A. (2005). Nanotechnology, nanomedicine, and the development of new, effective therapies for cancer. *Nanomedicine: Nanotechnology, Biology and Medicine, 1*(2), 101-109.

Khanna, V. (2012). Targeted delivery of nanomedicines. International Scholarly Research Network: Pharmacology, 2012, 1-9.

Labhasetwar, V. (2005). Nanotechnology for drug and gene therapy: The importance of understanding molecular mechanisms of delivery. *Current Opinion in Biotechnology, 16*(6), 674-680.

Nasongkla, N., Bey, E., Ren, J., Ai, H., Khemtong, C., Guthi, J., Chin, S., Sherry, A., Boothman, D. & Gao, J. (2006). Multifunctional polymeric micelles as cancer-targeted, MRI-ultrasensitive drug delivery systems. *Nano Letters, 6*(11), 2427-2430.

Nie, S., Xing, Y., Kim, G. J., & Simons, & J. W. (2007). Nanotechnology applications in cancer. *Annual Review of Biomedical Engineering, 9*(1), 257-288.

Ow, H., Larson, D., Srivastava, M., Baird, B., Webb, W., & Wiesner, U. (2005). Bright and stable core-shell fluorescent silica nanoparticles. *Nano Letters 5* (1), 113-117.

Peer, D., Karp, J., Hong, S., Farokhzad, O., Margalit, R., & Langer, R. (2007). Nanocarriers as an emerging platform for cancer therapy. *Nature Nanotechnology, 2*(12), 751-760.

Peng, G., Hakim, M., Broza, Y., Billan, S., Abdah-Bortnyak, R., Kuten, A., Tisch, U., & Haick, H. (2010). Detection of lung, breast, colorectal, and prostate cancers from exhaled breath using a single array of nanosensors. *British Journal of Cancer, 103*(4), 542-551.

Peto, R. (1983). The causes of cancer: Quantitative estimates of avoidable risks of cancer in the United States today. *The Use of Human Cells for the Evaluation of Risk from Physical and Chemical Agents, 66*(6), 587-593.

Phillips, E., Penate-Medina, O., Zanzonico, P., Carvajal, R., Mohan, P., Ye, Y., Humm, J., Gonen, M., Kalaigian, H., Schoder, H., Strauss, H., Larson, S., Wiesner, U., & Bradbury, M. (2014). Clinical translation of an ultrasmall inorganic optical-PET imaging nanoparticle probe. *Science Translational Medicine, 6*(260), 1-9.

Rahman, M., Hoh, B., Kohler, N., Dunbar, E., & Murad, G. (2012). The future of glioma treatment: Stem cells, nanotechnology and personalized medicine. *Future Oncology, 8*(9), 1149-1156.

Schnipper, L., Davidson, N., Wollins, D., Tyne, C., Blayney, D., Blum, D., Dicker, A., Ganz, P., Hoverman, J., Langdon, R., Lyman, G., Meropol, N., Mulvey, T., Newcomer, L., Peppercorn, J., Polite, B., Raghavan, D., Rossi, G., Saltz, L., Scjrag, D., Smith, T., Yu, P., Hudis, C., & Schilsky, R. (2015). American Society of Clinical Oncology Statement: A conceptual framework to assess the value of cancer treatment options. *Journal of Clinical Oncology, 33*(23), 2563-2577.

(2008). "What is Nanotechnology?" *Center for Responsible Nanotechnology*. Retrieved from http://www.crnano.org/whatis.htm.

(2016). "Cancer Facts & Figures 2016." *American Cancer Society*. American Cancer Society, Inc. Retrieved from http://www.cancer.org/acs/groups/content/@research/documents/document/ acspc-047079.pdf.